Advanced Interfacing Techniques for the Capacitive Sensors

Chapter · April 2017

DOI: 10.1007/978-3-319-55369-6_2

1 author:

Tarikul Islam
Jamia Millia Islamia
163 PUBLICATIONS **1,817** CITATIONS

Advanced Interfacing Techniques for the Capacitive Sensors

Tarikul Islam

Abstract Today, capacitive sensors are playing an important role in the measurement of different types of physical and chemical parameters. The capacitive sensor is very old and still it finds many new applications in different fields. Different types of the capacitive sensors and the interface electronics can be used for the instrumentation and the transduction application. The present chapter briefly reviews the important capacitive sensors suitable for the transduction applications. Some advanced electronic circuits for interfacing the perfect and the lossy capacitive sensors are discussed. The electronic circuits combine the advantages of the bridge method and the oscillator method of interfacing.

1 Introduction

The term "sensor" means to perceive something. The sensor represents the most important element in instrumentation, measurement and control applications. It is a device which senses the presence of the chemical or the physical parameters to be measured [1]. It is mainly used to collect different types of information from different sources which may be physical, chemical or biological in nature. Most often, the sensor converts any non-electrical quantity into an electrical signal. The transducer normally means a device, which converts the information from one form to the other form. The output energy of the transducer may be same or different from the input energy. According to the Instrument Society of the United States, the transducer is a device, which produces a measurable output in response to the specified physical or chemical measurand [2, 3]. A transducer is commonly called a passive transducer, if the output energy is almost entirely supplied by the input measurand while, an active transducer is one, which is having an auxiliary power

T. Islam (✉)
Jamia Millia Islamia, Central University, New Delhi, India
e-mail: tislam@jmi.ac.in

B. George et al. (eds.), *Advanced Interfacing Techniques for Sensors*,
Smart Sensors, Measurement and Instrumentation 25,
DOI 10.1007/978-3-319-55369-6_2

source, which supplies most of the power to the output signal [2]. On the other hand, an actuator acts opposite to a sensor, it generally receives the electrical signal and converts it into a nonelectrical signal. For example, a motor can be called an actuator [3].

The physical parameters to be measured by the sensors are generally pressure, force, inertia, acceleration, torque, temperature, humidity, flow, level, viscosity, displacement, speed, etc. The chemical parameters are of generally various toxic gases such as CO, NH_3, NO_2, toxic organic vapors, ionic concentration, chemical ware fare agents or biological species [1]. The sensors which work on the electrical effects can be fabricated utilizing different techniques such as resistive, capacitive, inductive, impedance, amperometric, electrolytic, ISFET, ChemFET, piezoelectric (SAW) etc. [1]. Among various types, the capacitive method is widely used for sensing a large number of physical and chemical parameters [2, 4–6]. For example, in automobile industry, practically all accelerometer sensors are of the capacitive type and most of the humidity sensors employ the capacitive method for humidity detection [2, 7, 8]. Similarly, many toxic vapors such as ethanol, methanol, isopropyl alcohol, etc. can be detected by the capacitive sensor [9, 10]. The main advantages of the capacitive sensor are easy fabrication, high sensitivity, low power consumption, small size and low cost [2, 4, 5]. However, toxic gases are normally detected by the resistive sensors and very recent, piezoelectric SAW devices get popularity day by day [1]. The present chapter mainly focuses on the capacitive type sensors and the recent advancement in the related electronic circuits. Three important classes of the capacitive sensors are used for the transduction applications [2, 6, 11–13]. These are

(a) Parallel plate capacitors
(b) Cylindrical co-axial capacitors
(c) Cylindrical cross-capacitors

Among them, the parallel plate capacitors are extensively used for the measurement applications [2]. The design of the capacitive sensor can be broadly classified into two categories: grounded and floating. In the grounded capacitive sensors, one of the electrodes of the sensor is connected to the ground terminal, while in the floating type capacitive sensors, neither of the electrodes are grounded [14].

2 Capacitive Sensors for Sensing Applications

2.1 Parallel Plate Capacitive Sensor

A parallel plate capacitor shown in Fig. 1 with the dielectric of permittivity ε_r can be expressed by the following expression [2, 11]

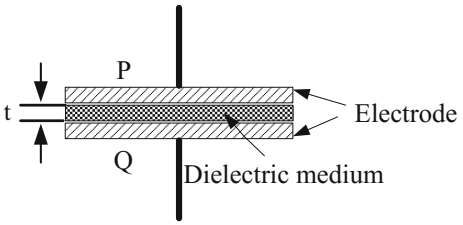

Fig. 1 Parallel plate capacitor

$$c = \varepsilon_0 \epsilon_r \frac{A}{t} \tag{1}$$

where 'A' is the cross-sectional area of the plate electrode, 't' is the gap between the electrodes. The expression (1) is true, when the gap between the electrodes is much smaller than the overlapping area. This is due to the fact that for t ≪ A, the fringing field is negligible. The capacitance (C) of (1) can be varied by (a) the cross-sectional area, (b) the gap between the electrodes and (c) the relative permittivity of the dielectric medium, (d) by inserting grounded plate between the stationary main Electrodes (4). Both the translation and the rotational motions can be measured by varying A and t. When the displacement is large, the gap is kept fixed and the capacitance variation due to the variation of A is preferred. But for smaller displacement, the area is kept fixed and the capacitance variation due to the variation of the gap is preferred. The capacitive sensor, which works on the variation of the gap is more useful for the transduction applications provided the variation of the gap is not large. The capacitance, with the gap variation can be given by [2]

$$c = \varepsilon_0 \epsilon_r \frac{A}{t + \Delta t} = \varepsilon_0 \epsilon_r \frac{A}{t\left(1 + \frac{\Delta t}{t}\right)} \tag{2}$$

The capacitance varies nonlinearly with the variation of t. In order to determine the linear range, expand the expression using Taylor series expansion,

$$c = \varepsilon_0 \epsilon_r \frac{A}{t}\left[1 - \frac{\Delta t}{t} + \left(\frac{\Delta t}{t}\right)^2 - \left(\frac{\Delta t}{t}\right)^3 + \cdots\right] \tag{3}$$

It is shown in the expression that for small change in gap, the change in C is directly proportional to the change in t. For example, in MEMS based sensor, the gap between the electrodes is of few μm only, so the proportionality can be maintained when Δt is ∼nm order [3]. The nonlinearity due to the gap variation can be eliminated by the use of the three electrode differential form of the structure as shown in Fig. 2. The sensor consists of three electrodes with air as the dielectric medium and forms two capacitances C_1 and C_2 with respect to the middle one. Both C_1 and C_2 can be varied either by moving the middle electrode keeping the outer

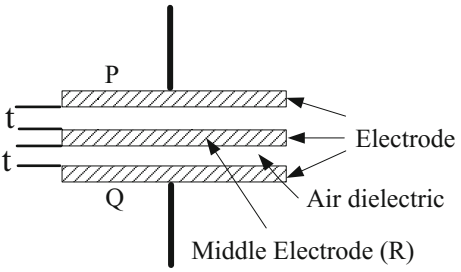

Fig. 2 Three electrodes parallel plate capacitor

electrodes fixed or by moving the outer electrodes keeping the middle one fixed. At the exact middle position, both the capacitances are equal. But if the middle electrode moves, one of the capacitances will increase, while the other will decrease. The capacitance C_1 and C_2 can be written as

$$C_1 = \varepsilon_0 \epsilon_r \frac{A}{t - \Delta t} \text{ and } C_2 = \varepsilon_0 \epsilon_r \frac{A}{t + \Delta t} \tag{4}$$

The differential form of the capacitance $C_d = (C_1 - C_2)$ for $(\Delta t^2 \ll t^2)$ can be written as

$$C_d = \varepsilon_0 \epsilon_r \frac{A}{t} 2 \frac{\Delta t}{t} \tag{5}$$

If we compare this expression with (2), the three electrode capacitor has linear relationship between C and delta t and the sensitivity is almost double. If one of the capacitances C_1 is excited by an alternating voltage source (V, ω) and the other by −(V, ω), then the current through the capacitor is given by

$$\mathrm{I} = \mathrm{j}\omega(C_2 - C_2)\mathrm{V} = j\omega \cdot \varepsilon_0 \epsilon_r \frac{A}{t} 2 \frac{\Delta t}{t} \cdot V \tag{6}$$

The current is proportional to the difference of two capacitances, which is proportional to the variation of the air gap due to the movement of the middle electrode. This current can be converted into a voltage signal using a current to voltage converter circuit. If the electrodes are fixed, then the three electrode capacitive structure can be used to measure the permittivity of the solid or the liquid dielectrics. For example, if C_1 is a free space air capacitor and C_2 is a capacitor with dielectric ε_r, whose permittivity is to be measured, then the permittivity of the dielectric medium can be given by the following expression [15]

$$\varepsilon_r = \frac{C_2}{C_1} \tag{7}$$

Thus, the permittivity can be determined by taking the ratio of the two capacitances. Sometimes, there is a need to fabricate a multi dielectric capacitive sensor

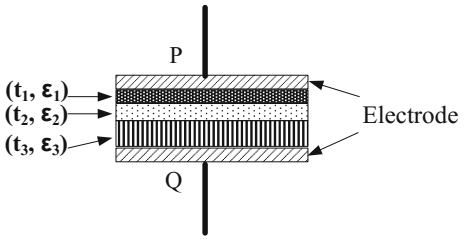

Fig. 3 Multi dielectric parallel plate capacitor

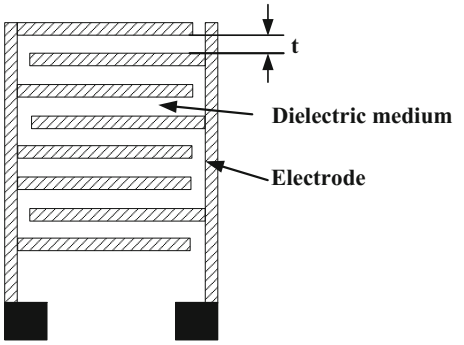

Fig. 4 Interdigitated (multi-electrode) capacitor

for sensing the measurands. For a parallel plate capacitive sensor with multiple dielectric layers shown in Fig. 3, the capacitance value can be represented by [11].

$$\frac{1}{C} = \frac{1}{C_1} + \frac{1}{C_2} + \frac{1}{C_3} = \frac{A}{\frac{t_1}{\varepsilon_1} + \frac{t_2}{\varepsilon_2} + \frac{t_3}{\varepsilon_3}} \tag{8}$$

where t_1, t_2, t_3 are the thickness of the dielectric layers of permittivity ε_1, ε_2, ε_3 respectively. For example, a capacitive humidity sensor fabricated by depositing the moisture adsorbing metal oxide film on the polyimide substrate, the resulting capacitor structure with multiple dielectrics is formed. Such sensor is employed to measure the humidity over a wide dynamic range [16].

Another interdigitated parallel plate (IDT) capacitive structure, which is very popular in the literature for humidity and organic vapors sensing is shown in Fig. 4. This is a multi-electrode capacitor fabricated on the dielectric medium [17, 18]. For an interdigitated electrode capacitor with permittivity ε_r having N number of plates (fingers), the capacitance can be approximately (electrodes are close to each other) given by

$$C = \frac{\varepsilon_0 \varepsilon_r (N-1)}{t} \tag{9}$$

The equation shows that the capacitance of the parallel plate capacitor can be increased to a large value by using the multi plates with identical dielectric. The number of plates on both sides of the capacitor may be same or be different. Some

interdigitated capacitors with guard electrode are also reported in the literature [19]. The capacitive sensor based on the change in relative permittivity is most often used for sensing the humidity and the organic vapors or determining the dielectric constant of the dielectric materials or detecting the biological species [20]. For sensing the water and the organic vapor molecules, the sensing film is deposited either on the IDT or below the IDT.

2.2 Cylindrical Coaxial Capacitive Sensor

This is another useful capacitive structure for the sensing application. The most practical example of the coaxial cylindrical capacitor, is the coaxial cable. Consider two concentric conducting cylinders separated by the dielectric medium ε as shown in Fig. 5a. The outer diameter of the inner cylinder is d meter and the inner diameter of the outer cylinder is D meter. The expression of the capacitance with the cylinder length L is [11]

$$C = \frac{2\pi\varepsilon L}{ln\frac{D}{d}} \tag{10}$$

Such structure can find application for the measurement of non-conducting liquid level or other parameters [21, 22]. The structure for the measurement of the non-conducting liquid level using the cylindrical sensor is shown in Fig. 5b. Suppose, the length of the cylinder is L meter and the level of the liquid is H meter, then the capacitance for determination of the liquid level can be given by following expression

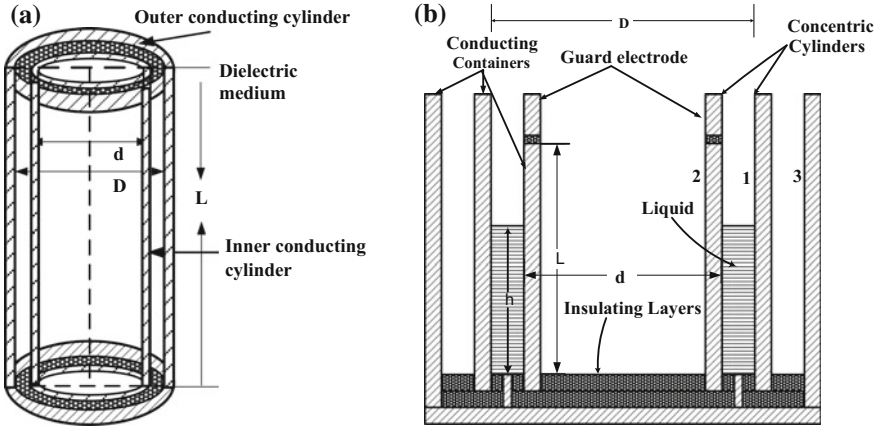

Fig. 5 **a** Cylindrical coaxial capacitor. **b** Coaxial capacitor for liquid level measurement

$$C_{12} = 2\pi \frac{[H\varepsilon_r + (L-H)\varepsilon_{r1}]}{ln\frac{D}{d}} \tag{11}$$

where, ε_r and ε_{r1} are the permittivity of the liquid and air respectively. The (11) can be written as

$$C_{12} = KH(\varepsilon_r - 1) + KL \tag{12}$$

where $K = \frac{2\pi}{ln\frac{D}{d}}$. Thus, the capacitance is directly proportional to the level of the liquid.

2.3 Cylindrical Cross-Capacitor

This is another very useful capacitive structure which is used as a primary standard due to its single dimensional accuracy. Consider a cross-section of a conducting cylinder of length L in a dielectric medium ε shown in Fig. 6. The cylinder is divided into four equal parts (A, B, C, D) with very small insulating gaps at points (a, b, c, d) [6].

The cross-capacitances (C_1, C_2) between the opposite parts A-C and B-D can be given by

$$e^{-\frac{C_1\pi l}{\varepsilon 0}} + e^{-\frac{C_2\pi l}{\varepsilon 0}} = 1 \tag{13}$$

For $C_1 = C_2 = C_0$, then $C_0 = \ln(2)L$.

In a well-designed cross-capacitor, $C_1 = C_2$ can be easily achieved. However, if there is a deviation from the symmetry, C_0 will differ from C_1 or C_2 by ppm only.

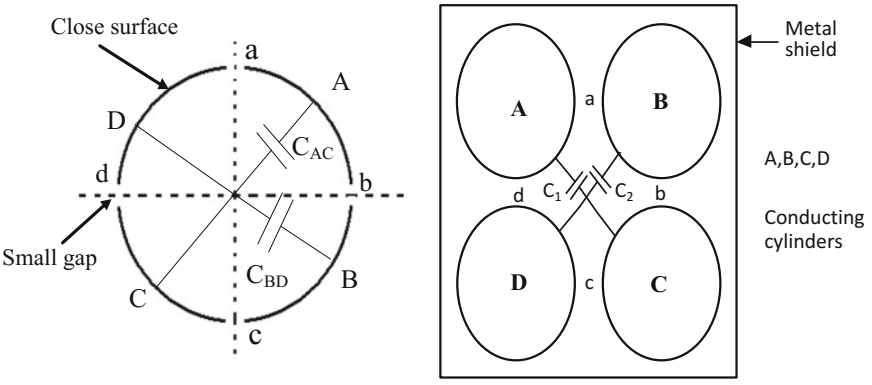

Fig. 6 Cylindrical capacitors with metal shield

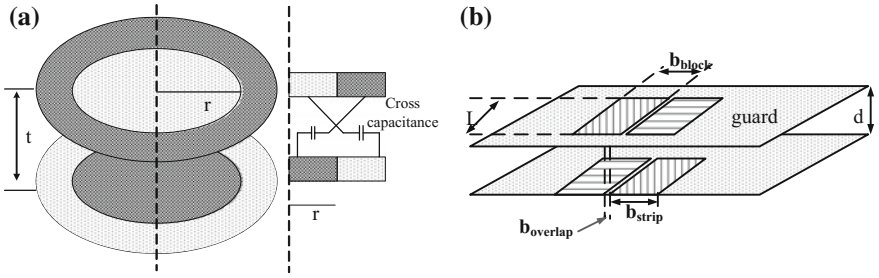

Fig. 7 The cross-capacitor **a** circular **b** strip sheet planar

The most important advantage of the cylindrical cross-capacitance is that the capacitance value can be determined by a single length measurement. Therefore, the accuracy of the capacitor depends on the accuracy of the length measurement only. However, the structure proposed by the Thomson and Lampard is not suitable for sensing application as the materials and the fabrication of the structure are costly. Also the capacitance value is small, unless the length is larger. Rahman and VGK Murty utilize the cross-capacitive structure for the measurement of the pressure [22]. An alternative structure as suggested by the Heerens [12, 13] shown in Fig. 7a is more suitable for the fabrication and may be useful for the sensing applications.

When r $\gg$ t, the capacitance value C is given by the following expression [12]

$$C = \frac{\varepsilon_0 \varepsilon_r \ln(2)}{\pi} 2\pi r \left[1 + 0.00043507\left(\frac{t}{r}\right)\right] - 0.050631437\left(\frac{t}{r}\right)^2 + \cdots \tag{14}$$

The analytical calculation of the circular structure is complex and the numerical solution based on the finite element method does not give desired accuracy. This circular capacitor can be replaced by a lateral strip type capacitor. This strip sheet capacitor shown in Fig. 7b can be treated as the transformation of the circular cross-capacitor having guard electrode with infinite radius r [12].

The cross-capacitance of the strip sheet capacitor can be given by

$$C \cong \frac{\varepsilon_0 \varepsilon_r}{\pi} L \left(\ln(2) + ln\left(\cosh \frac{\pi b_{overlap}}{2d} \right) \right) \tag{15}$$

However, this capacitor is less symmetrical and hence, the sensitivity to the parameter variations may be comparatively more than the circular cross-capacitor. Fabrication of the strip capacitor is easy and may be useful for the precise measurement of some of the measurands.

3 Precautions Necessary for the Use of the Capacitive Sensors

3.1 Shielding of the Capacitive Sensor

For the capacitive type transducer for sensing applications, most of the times, it is absolutely necessary to shield the capacitors from the external electrostatic fields. There are different sources, which produce the unwanted electrostatic field [6, 11]. Shielding is provided by enclosing the capacitor inside a grounded conducting metal. The conducting shield may be made of aluminum, copper, brass or the wire mesh [11]. Due to the presence of the shield, the charges accumulated on the shield pass to the ground without affecting the overall capacitance value of the capacitors. However, in one of the research papers, the metal shield of a three-electrode capacitor has been used for the measurement of the speed of a rotating device like motor [23]. A parallel plate capacitor within a metallic shield can be represented by a three-terminal capacitor as shown in Fig. 8a. C_{AB} is the actual desired capacitance, C_{AG}, and C_{BG} are the parasitic capacitances formed at terminals A and B respectively with respect to the grounded metal shield. C_{AG}, and C_{BG} can be minimized by selecting a suitable circuit configuration of an interfacing electronic circuit as reported in [4, 10, 15].

3.2 Guarding of the Capacitor Electrodes

To avoid the inaccuracy in the calculation of the parallel plate capacitor due to the fringing fields at the edges of the electrodes, the guarding is necessary [11]. The distribution of such unwanted fields is uncertain and this causes, an inaccuracy in the exact value of the capacitance. Figure 9 shows the arrangement of a guard ring of a parallel plate capacitor. The ring, which surrounds the electrode P of the capacitor is of the metallic plate. The thickness of the guard ring may be of the same plate thickness P. There is a small gap between the guard ring and the plate P. The outer diameter of the guard ring is usually same as the diameter of Q, the other plate of the capacitor.

If the guard ring is the same potential as that of the electrode P, then the fringing field is transferred to the extreme edges of the guard and in this situation, the effective area of the capacitor is now equal to the electrode of the plate P. The guard electrode is essential for other types of the capacitive sensors such as the cylindrical coaxial and the cylindrical-cross capacitor including the structure proposed by Heerens [12]. For the cylindrical capacitor, the guard ring is also in cylindrical shape and of the same diameter as that of the cylindrical electrode to which the guard is attached. It is placed at one end and is coaxial to the cylindrical electrode. In the cylindrical capacitor shown in Fig. 5b, for the liquid level measurement, the guard ring is coaxial and placed at one end of the inner electrode.

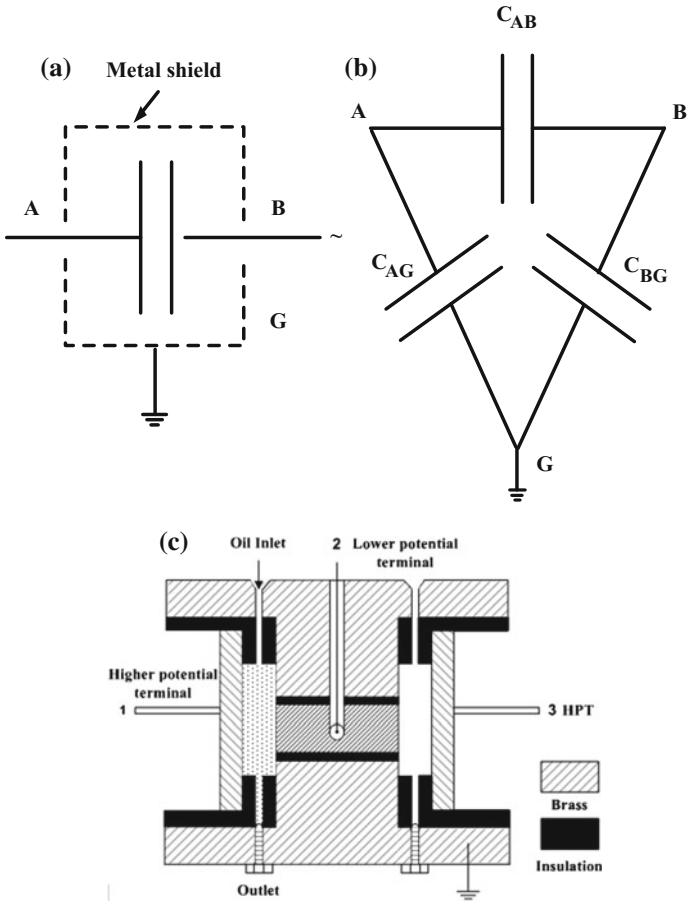

Fig. 8 Capacitor **a** within a grounded metal shield, **b** equivalent circuit, **c** three electrode capacitors within metallic shield

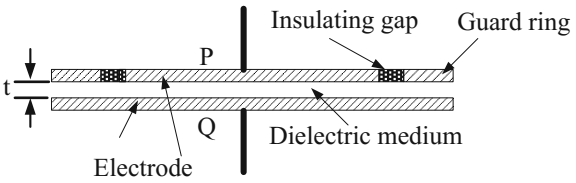

Fig. 9 Parallel plate capacitor with guard ring

3.3 Shielded Cable and the Cable Length

These are other important precautions necessary for the capacitive sensors. These requirements are more stringent for the low value capacitive sensors. The

connecting wire is essential every time the sensor is to be interfaced with the detection electronic circuit. Normally, the cable is having two insulated wire, which has an unnoticed distributed wire capacitance along its length. The wire capacitance depends on the type of the insulation of the conducting wires and the length. This capacitance is combined with the desired sensor capacitance. The typical value of the wire capacitance is 30 pF/ft and the resistance is of 0.01 Ω. One solution is to use the shielded cable, which is having the metallic mesh or the thin sheet on the outer periphery of the insulated signal wire. This grounded metallic shield prevents the external electrostatic field to couple with the wire. However, the metal shield is not effective to prevent the electromagnetic noise without magnetic shielding. Magnetic noise picks up can be reduced by using a twisted signal wire (minimize loop area). A commercially shielded cable is having twisted wires wrapped within a metal shield. However, the internal distributed capacitance between the signal conductors can be reduced by insulating the wires with high quality insulation like Teflon and by reducing the length of the wire as far as possible [2]. Also, it is important to avoid the formation of the ground loop, when the interface circuit is connected to more than one ground point.

4 Lossy Capacitive Sensor

When a capacitor is excited by a constant DC voltage source of V volts, the charging current flows through the capacitor for a short duration of time till the capacitor is charged to the full voltage. The current through the capacitor stops flowing, when the voltage, across the charged capacitor reaches the input voltage level. A small conduction current continuously flows through the capacitor due to the presence of very high resistance of the dielectric medium. But, it is observed in practice, in most of the dielectrics, the initial charging current is much higher than the conduction current and the current decays exponentially taking longer duration to stop. This suggests, the other phenomena like the adsorptive nature of the dielectrics. If a capacitor with an absorptive dielectric is initially charged, and then discharged, it charges itself and the potential across its plates rises again. This absorptive behavior is due to the viscous movement of the ions and the molecules in the dielectrics.

Initially, when a capacitor is connected across a voltage source, the ions and the molecules move very fast for a short duration of time giving rise to large initial charging current, but later on due to slow motion, the current takes longer times. For an absorptive capacitor, the time response of accumulation of the charges is shown in Fig. 10a [10]. The time response of the charges Q consists of three important parts: (i) the initial high charging current (ii) slowly rising absorptive current and the steady state conduction current. An absorptive capacitor can be approximately represented by an equivalent circuit shown in Fig. 10b. C is the geometric capacitance due to the permittivity of the dielectric medium, R_b is the resistance of the dielectric contributing the conduction current and (C_a, R_a) are

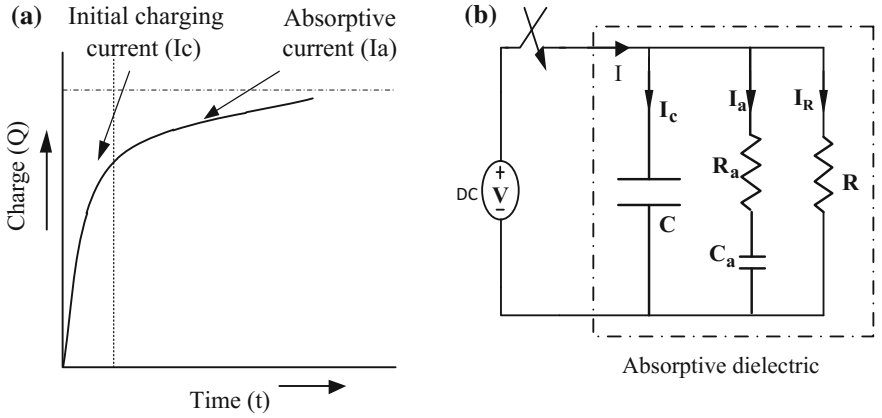

Fig. 10 **a** Time response of charge accumulation in the absorptive capacitor, **b** its equivalent circuit

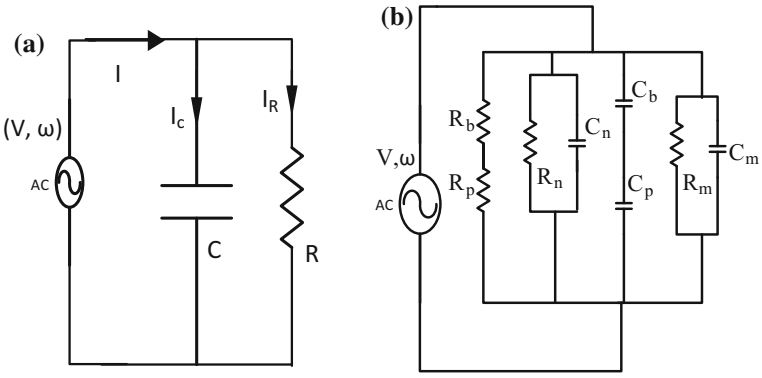

Fig. 11 **a** AC equivalent circuit of a lossy capacitor, **b** equivalent circuit of an Al_2O_3 moisture sensor

the resistance and the capacitance contributing the absorbing current. In an actual capacitor, there may be several such branches of (C_a, R_a) in the equivalent circuit.

When the capacitor is connected across an alternating voltage source V (rms), the absorption effect causes the power loss. The current I (rms) through the dielectric leads the voltage by angle Φ. This angle is equal to 90° for the perfect capacitive sensor but for the lossy capacitor, it is less than 90°. The loss angle δ is equal to (90 − θ)°. The dielectric loss is given by VIcosΦ or IVsinδ. An imperfect capacitor at any signal frequency can be equivalently represented by a perfect capacitor in parallel with a resistance showing the power loss (Fig. 11a). The equivalent resistance in general varies with the frequency. For example, a humidity sensor or an organic vapor sensor works as a lossy capacitor. The capacitance and

the resistance of the sensor vary with the signal frequency [11, 18]. The power loss in the imperfect capacitor can be given by $P = V^2\omega C\tan\delta$.

For example, consider a porous aluminum oxide capacitive humidity sensor. The porous oxide is formed by anodization of a pure aluminum sheet in the presence of acidic electrolytic solution (sulphuric or oxalic acid). Anodization is one of the well-established methods to prepare the nanostructure of the metal oxide, which is used for the measurement of the humidity over a wide dynamic range from %RH to trace moisture in ppm level. The approximate equivalent circuit of the metal oxide humidity sensor is shown in Fig. 11b [24]. In Fig. 11b, C_n, R_n are the capacitance and the resistance of the alumina nano-walls, C_p, R_p are the capacitance and the resistance of the void (pores), C_m, R_m denote the multi-dielectric (barrier layer, chemisorbed layer, water condensed in the voids) capacitance and resistance respectively.

5 Advancement in the Design of Electronics Interface for the Capacitive Sensors

5.1 Introduction

An interface electronics or read out is a detection electronic circuit, which is designed and realized according to the type and the output of a primary sensing element. Sensors and the detection electronics are the most important parts of a measurement system. Performance of a measurement system is generally specified by accuracy, repeatability, sensitivity, resolution, linearity, response and recovery times, hysteresis, drifts, cross-sensitivity [1]. The functional units of a sensor are based on measurement system in general, and can be represented by the following block diagram (Fig. 12).

The primary sensor/the transducer senses the presence of the desired physical or chemical parameter to be measured. The output of the sensor may or may not be in a suitable form for further processing. The sensor may be either the resistive or the inductive or the capacitive type, sometimes, it provides the output in the form of the voltage or the current signal. Most often, the desirable output of the electronic circuit is to be in the form of voltage, current or frequency (time period). Since, the real world phenomena are continuous in time, the output of the sensor is analog. However, the digital output of the sensor is desirable for easy interfacing, noise

Fig. 12 A general block diagram of a measurement system

immunity, storing and communication with a digital system. The parameters of the sensor can be measured by a LCR meter, but for a low cost dedicated electronic test system, the interface electronic circuit is needed. The interface circuit provides an easy manipulation and the conditioning of the electrical signal such as amplification, filtration, minimization of loading effects, (impedance matching) etc. When, the sensor is remotely placed to monitor the measurand, it is necessary to transmit data. Finally, the data should be represented in the form, which can be easily displayed (analog or digital), recorded and stored. The signal conditioning unit is another important unit in the measurement system. When a sensor is to operate in a particular environment, there are some undesired inputs which invariably affect the desired output signal causing significant measurement error. One of the inputs may be called interfering input, which is often present in the environment such as 50 Hz electromagnetic fields or electrostatic fields generated by the nearby electrical apparatus. The ambient temperature or the humidity may be treated as other interfering input. Sometimes, a situation becomes worse, when the interfering input modifies the input–output relation of the desired signal. Therefore, care must be taken to avoid the errors to ensure the correct measurement accuracy.

Different interface electronic circuits, based on resonant oscillators, AC bridge, charge–discharge, capacitance to frequency (or time period) or capacitance to phase angle have been reported in the literature to interface the different capacitive sensors [25–28]. The suitability of the techniques for the measurement applications depends on the requirement of accuracy, resolution, minimum baseline drift, immunity to the stray capacitance, effects of humidity and ambient temperature and elimination of the shunt conductance of the sensor [25]. The resonant method is very old and effective for measuring both capacitance and conductance of the sensor. In this, an unknown capacitor is a part of a resonant circuit, which is having known value of the inductance. The resonance condition is obtained by varying the input signal frequency and is detected either by measuring the voltage or the current. The capacitance and the resistance of the sensor are measured from the expression derived at the resonant condition. This method is rarely used nowadays because of manual adjustment of the frequency of the source voltage for obtaining the resonant condition and the difficulties of minimizing the stray effects [25].

In the charge-discharge method, the sensor capacitance is charged with a fixed voltage V using an analog switch and then discharged through a current detector using a second switch. The charge-discharge steps are repeated for several cycles (f) with the controlled clock pulse. The average discharge current ($=V\ f\ C_x$) is then converted into a DC voltage. For better accuracy and the minimization of the conductance of the capacitor, sometime differential configuration having another identical charge–discharge network with reference capacitance C_r is employed. However, it also suffers from poor immunity to the stray capacitance effect [25].

The AC bridge method is still considered as the most accurate and stable method for interfacing a capacitive sensor, which is having small capacitance change [25, 26]. The bridge consists of four arms formed by unknown impedance, reference impedance, and two out of phase identical voltage sources. If the two impedances are not in balance, an imbalance current flows through the bridge which can be

converted into a voltage signal using a current to voltage converter (I-V). This is immune to various sources of the errors, including the most prominent stray capacitance. A phase detector circuit at the output of the I-V converter reduces various sources of the noise, thus giving highly sensitive and accurate results. The accuracy can be further improved by incorporating an auto balancing arrangement to minimize the fluctuation of the excitation voltage. By auto balancing of the bridge, the capacitance value lower than pF can be measured [29, 30]. The main drawback of the AC bridge is the limited measurement range of the capacitance value [25].

In the oscillation method, the unknown capacitance C_x is the part of an LC or RC oscillator circuit [25, 26]. The oscillation frequency (or time period) depends on the value of the C_x, therefore, by measuring the frequency, the capacitance value can be determined. Nowadays, the relaxation oscillator based interface electronics are getting popularity day by day for both capacitive and resistive sensors [31–36]. This method is suitable for interfacing the sensor, whose capacitance value varies over a wide range. However, the oscillation method suffers from poor immunity to the stray capacitance, the frequency stability and the effects of the shunting conductance. There are some commercially available evaluation boards ICs which can be used to directly interface the capacitive sensors like analog device AD7746, Texas Instrument FDC1004EVM [37]. These evaluation boards are capable of measuring very small capacitance with Femto farad resolution, but these boards do not provide much flexibility to the user for different type of the capacitive sensors and are costly.

5.2 *Interface Electronics Circuit for the Capacitive Sensors*

A simple opamp based interface read out for a capacitive sensor is shown in Fig. 13a. Often a large value resistance is connected across the feedback

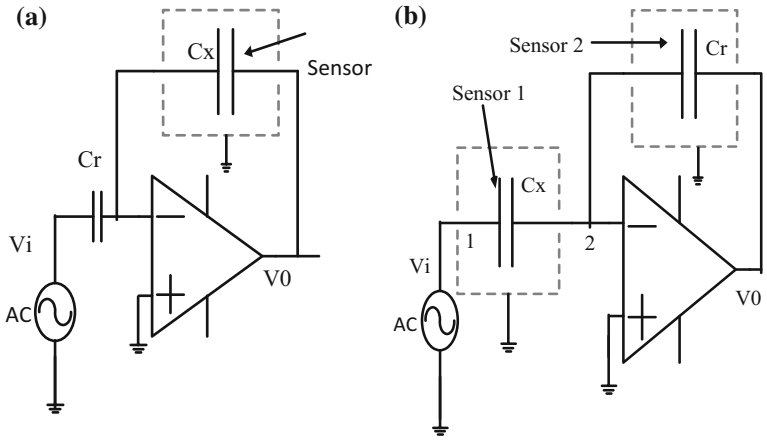

Fig. 13 The simple interface circuit using opamp as inverter **a** single sensor **b** double sensors

capacitance to provide a path for the DC current due to the opamp offset voltage and the DC bias current. Assuming ideal opamp, the voltage output can be given by [2]

$$V_0 = -V_i \frac{C_r}{C_x}, \text{ or } V_0 = -V_i \frac{t}{A} \frac{1}{\in_0 \in_r} C_r \tag{16}$$

The output voltage is directly proportional to the gap (t) between the electrodes of the senor. The output voltage can be directly calibrated into the motion of the moving plate. If C_x and C_r are the two identical air capacitors with a common electrode (terminal 2), the inverting opmap configuration shown in Fig. 13b can be used to measure the relative permittivity (ε_r) of the dielectric medium [15, 38]. Such three-electrode capacitive transducer is shown in Fig. 8c. For example, if C_r is the capacitance with a dielectric medium and C_x is the free space air capacitor, then Eq. (16) can be written as

$$\begin{aligned} &V_0 = -V_i \in_r \\ &\text{since } C_r = \frac{\in_0 \in_r}{t} A \text{ and } C_x = \frac{\in_0}{t} A \end{aligned} \tag{17}$$

Thus, the output voltage of the interface is directly proportional to the permittivity of the dielectric medium to be measured. The circuit may be suitable for the precise measurement of a capacitance with the immunity of the stray capacitance. If the capacitive sensor is within a conducting grounded shield as shown in Fig. 8a, then it can be represented by an equivalent circuit as shown in Fig. 8b. C_{2G} and C_{1G}, are the parasitic capacitances. Output voltage V_0 of the interface circuit will be almost independent of the stray capacitances. This is because, the stray capacitance C_{1G} appears across the input voltage and the node 2 is at the virtual ground potential, therefore C_{2G} will be negligible. The same inverting opmap based interface circuit can also be utilized to interface a lossy capacitive sensor like porous silicon/porous alumina/polymer based humidity sensor. The amplitude or the phase angle of the output voltage signal of the inverting configuration will vary according to the variables. The circuit based on the phase detection principle with input signal V_i is shown in Fig. 14. The possible waveforms at different terminals of the circuit are shown in Fig. 15. The phase angle of the opmap output V1 is shifted due to the change in impedance (Zx), caused by the measurand for example, the humidity. The phase change of the output signal (V1) with respect to the input signal (Vi) can be extracted by converting both the input and the output signals to the square wave outputs using the comparators and then by comparing the outputs by a digital XOR gate. The output of the XOR gate is a pulse wave signal, which can be converted into a DC voltage (V_{DC}) using a demodulator or into the proportional clock pulses [39].

In Fig. 14, $Z_x (= R_x \| C_x)$ is a capacitive sensor at the input and $Z_f (= R_f \| C_f)$ is the impedance at the feedback path of the opmap respectively. The output V_1 at the output of the inverter is given as $V_1 = -V_i Z_f Y_x$, where the admittance

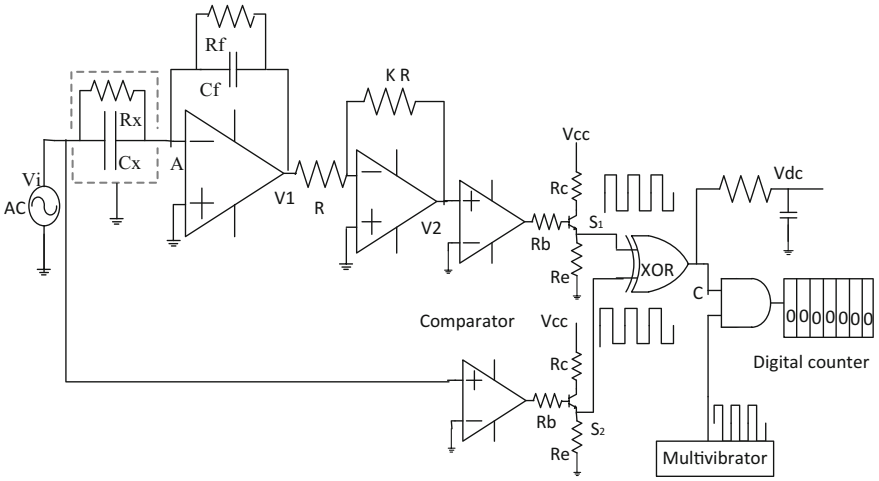

Fig. 14 Opamp configuration to interface a lossy capacitive sensor

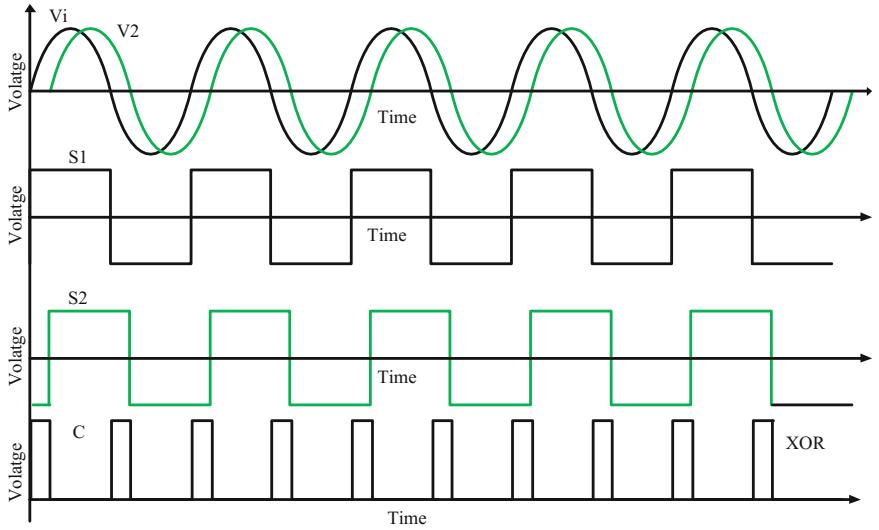

Fig. 15 Timing diagram at different points of the circuit

$Y_x = \frac{1}{Z_x} = G_x + j\omega C_x$ and the impedance $Z_i = \frac{R_f}{1+j\omega C_f R_f}$, $G_x\left(=\frac{1}{R_x}\right)$, ω is the signal frequency $(=2\pi f)$. The output of the second stage inverter, $V_2 = V_i Z_f Y_x$, which can be written in polar form as

$$V_2 = KV_m|Z_f||Y_x|\angle(\omega t + \theta_1 - \theta_2) \tag{18}$$

where $|Y_x| = \sqrt{G_x^2 + \omega^2 C_x^2}$, $\theta_1 = \tan^{-1}\omega C_x R_x$, $|Z_f| = \frac{R_f}{\sqrt{1+\omega^2 C_f^2 R_f^2}}$, $\theta_2 = \tan^{-1}\omega R_f C_f$, V_m is the peak amplitude of the excitation voltage. The output, V_2 and the input V_i are applied to the comparators to get square wave signals 'S_1' and 'S_2' then scaled by the transistor. Finally, both the square wave signals are applied to the XOR gate, the output of which is a pulse wave signal 'C'. The output of the XOR gate is digitally ANDED with high frequency stable clock pulses from the output of the multivibrator. The output of the AND gate is then applied to a digital counter to obtain the digital word that represents the phase angle [39]. The circuit was simulated using circuit simulation software and then was hardware implemented on the breadboard. For hardware implementation, the active components use are Op-07, comparator LM339, transistor 2N2222, XOR gate 74LS136 and AND gate 74LS11. The circuit was excited by a source voltage of 1 V(rms) and 1 kHz frequency. Initial experiments were performed using discrete resistance and ceramic capacitance for Z_x and C_f = 100 pF, R_f = 1 MΩ for Z_f. Suitably scaled square wave signals using transistors 2N2222 are applied to the inputs of XOR gate with the help of a digital buffer (74LS244). The output of the XOR gate along with the high frequency clock pulses is applied to the AND gate. Schmitt trigger circuit realized using CD40106B generates a 500 kHz clock frequency signal. Finally, the digital counter CD4029 counts the clock pulses and seven segment display unit displays the counted pulses.

Table 1 shows the counter output for the variation of the capacitance in the pF range. The counter output increases almost linearly with the increase in the capacitance value. The sensitivity and the resolution of the interface can be increased further by using high frequency clock pulses and utilizing the fast opamps for the comparator. The accuracy of the interface was analyzed for three different sources of errors such as (i) offset voltage (ii) error due to rising and falling edge of XOR gate output and (iii) the parasitic earth capacitance. The circuit was used to interface different types of humidity sensors for measuring the humidity from % RH to trace moisture in ppm level. Tables 2 and 3 show the responses of the circuit for the porous alumina and porous silicon (PSi) based humidity sensors. The

Table 1 Response of the circuit for the discrete capacitance

Vi = 1 V, f = 1 kHz, R_x = 980 kΩ							
Capacitance (pF)	100	150	200	250	300	350	400
Counter output	2	5	8	10	11	13	15

Table 2 Response of the interface circuit for PA humidity sensor

Humidity (%)	11	25	45	70	83	97
Counter output	20	27	38	52	57	59

Table 3 Response of the interface circuit for PSi humidity sensor

Humidity (%)	11	25	45	70	83	97
Counter output	21	23	25	28	32	34

effectiveness of the interface to the lossy capacitive sensor is clearly visible. However, the interface uses a single sensor may suffer from the baseline drift and the effect of the ambient temperature.

5.3 Oscillator Based Transformer Ratio Arm Bridge for Interfacing the Capacitive Sensor

The transformer bridge based AC bridge method is one of the oldest and accurate techniques to measure the small capacitance. The AC bridge method has limited capacitance measurement range. The oscillator based interface is popular for interfacing the wide range capacitive sensor. If both the AC Bridge and the oscillator based methods are combined, it is possible to measure the capacitance of a sensor accurately with a wide measurement range. Therefore, in the present circuit, AC bridge and oscillator has been combined to improve the range and the measurement accuracy of the capacitive sensor [40].

5.3.1 Working of the Interface Electronic

Figure 16 shows the interface circuit. Part 1 enclosed within a block is the transformer ratio arm bridge circuit (TRA) realized using an audio frequency centre tap transformer. The primary of the transformer is excited by the output of a relaxation oscillator and the secondary of the transformer generates two 180° output of phase signals (V_i and $-V_i$). The secondary outputs of the TRA are connected to the reference capacitance C_r and the sensing capacitor C_x respectively. (C_{p1} and C_{p2}) and (C_{r1} and C_{r2}) are the stray capacitances of C_x and C_r. C_{p1} and C_{r1} capacitances that appear across the voltage sources of the transformer secondary and $(C_e = C_{p2} + C_{r2})$ is the parasitic capacitance at the detector terminal D, which is at the virtual ground potential. The stray capacitances have negligible effects on the output voltage V_{01} of the opamp A1 because of minimum voltage source impedance and the virtual ground potential at point D. The unbalance detector current I_D, which is proportional to the difference of the capacitance ($C_r - C_x$) is converted into the voltage signal V_{01} using a current to voltage converter circuit. Part 2 is the relaxation oscillator circuit consisting of an integrator and a Schmitt trigger (hysteresis comparator). The output V_{01} of the TRA bridge with a buffer is applied to one of the inputs of the integrator and the other input of the integrator is the output of the comparator V_C. The output of the integrator is connected to the positive input

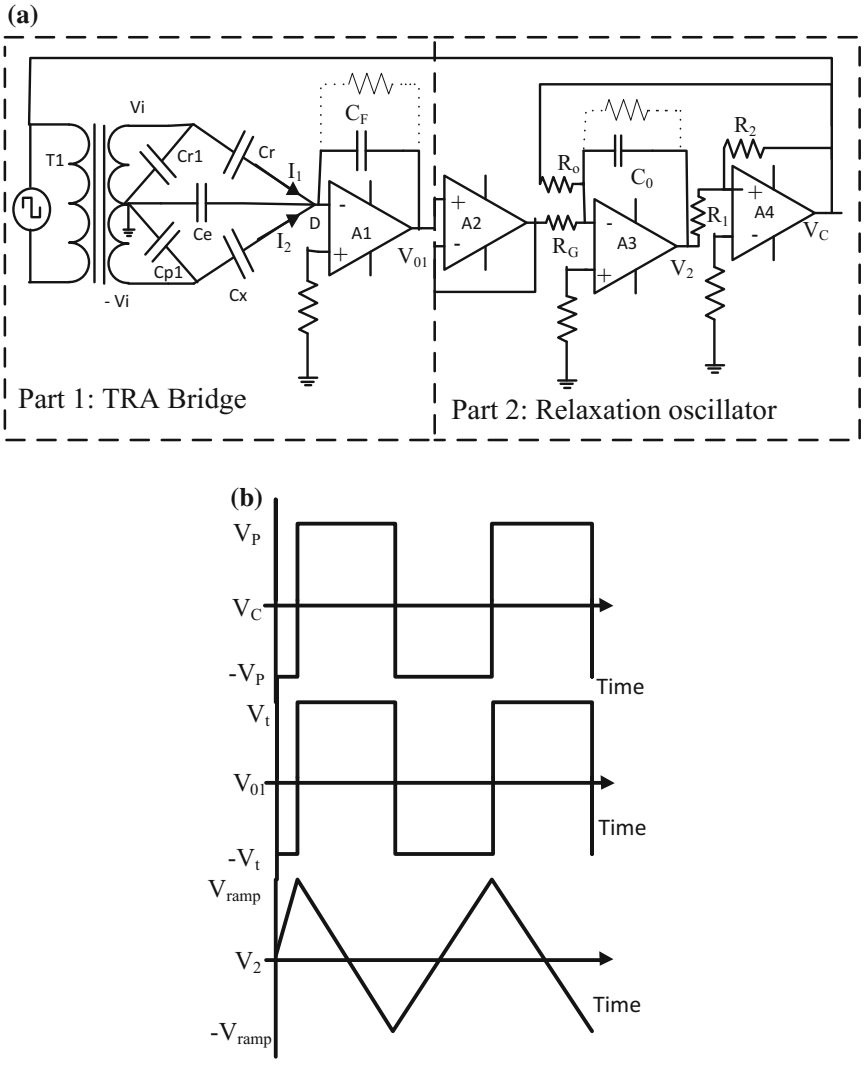

Fig. 16 **a** Schematic diagram of the signal conditioning circuit. **b** Significant waveforms at the different output terminals of the circuit

terminal of the comparator. The V_{01} output of the TRA bridge, at unbalance condition in the time domain can be given by

$$V_{01} = -\left(j\omega C_r V_i - j\omega C_x V_i\right)\frac{1}{j\omega C_F} \text{ or, } V_{01} = \left(\frac{C_x - C_r}{C_F}\right)V_i \tag{19}$$

5.3.2 Capacitance to Frequency Converter

When the peak of the comparator voltage output $|+V_p| = |-V_P| = V_C$ is symmetrical, the output voltage of the integrator is a triangular wave with V_2(p-p) is $2\frac{R_1}{R_2}V_c$, which is set by the Schmitt trigger circuit (comparator hysteresis) [19, 26]. During an unbalance of TRA bridge condition, the frequency of the output signal can be given by

$$f = f_0\left(1 + \frac{R_0}{R_G}\eta\delta\right) \tag{20}$$

where, the central frequency at the balance condition $f_0 = \frac{R_2}{4R_0C_0R_1}$, $\delta = \frac{C_x - C_s}{C_f}$, and η is transformation ratio of the transformer ($\eta = V_i/V_C$). When the capacitance of the sensor C_x in presence of measurand changes to $C_x + \Delta C_x$, then the frequency of the output signal can be written as

$$f = f_0\left(1 + \frac{R_0}{R_G}\eta\frac{\Delta C_x}{C_f}\right) \tag{21}$$

Thus, the change in the frequency is directly proportional to the change in the capacitance of the sensor. Simulation work has been performed with the help of the equivalent circuit of the bridge to study the frequency error due to the stray capacitance and the effect of the temperature of the sensor. Errors due to the offset voltage of the opamps, fixed time delay of the comparator, and the components values are also analyzed [40]. The circuit provides satisfactory results.

5.3.3 Hardware Realization of the Circuit and Determination of the Response Characteristics of the Humidity Sensor

The circuit was implemented using a high slew rate and fast response opamp LF-351. The central frequency f_0 is selected to be at 11.4 kHz for the response of a capacitive moisture sensor. The component values are: $C_0 = 0.954$ nF, $R_0 = 0.232$ MΩ, $R_1 = 0.978$ kΩ, $R_2 = 9.89$ kΩ, $R_G = 35$ kΩ and $C_F = 100$ pF. For the TRA bridge, an audio frequency centre tap transformer with transformation ratio $\eta = 1/20$ for the generation of the secondary voltage ($\pm V_i$) of 1.18 V has been employed. Both the primary and the secondary windings are placed on the high permeability core. The interface was initially tested with discrete ceramic capacitances and the variable gang capacitors and finally with the capacitive humidity sensor. C_r is a reference capacitance and C_x is an unknown variable capacitance arm. The output voltage V_{01} has been measured by varying the capacitance C_x with values $C_r < C_x$. Table 4 shows the values of V_{01} for different values of C_x with $C_r = 110$ pF (fixed). It shows that the output voltage proportionally increases with an increase in the difference ($C_x - C_r$) almost linearly with slop 0.0082 V/pF.

Table 4 Output voltage V_{01} with change in the capacitance C_x

C_r = 110 pF (fixed)									
Cx (pF)	110	134.3	177.4	199.2	218.6	233.7	247.7	261.7	279
V_{01} (V)	0.13	0.32	0.66	0.82	0.96	1.08	1.18	1.28	1.42

Table 5 Frequency (f) with the variation of the capacitance C_x

C_x (pF)	8.38	20.29	37.14	59.1	86.82	112.7	134.3	199.22
f (kHz)	3.94	4.486	5.02	6.14	7.37	8.58	9.60	12.43

Table 6 Reading of the prototype moisture meter

Commercial moisture meter (ppm)	21	39	56	63	101	108
Prototype meter moisture (ppm)	20	39	54	62	100	107

Change in frequency of square wave output of the interface measured using a digital oscilloscope (Agilent Technologies DSO1002A) with the discrete ceramic capacitance at the central oscillator frequency of 3.95 kHz is shown in Table 5.

The interface was successfully utilized to develop a prototype digital hygrometer using a laboratory fabricated trace moisture sensor [40–43]. For the development of the meter for the moisture measurement, the output of the oscillator is interfaced with a PIC microcontroller. The microcontroller was programmed in the timer mode to measure the frequency. The frequency values are calibrated in-terms of the moisture. The nonlinearity of the frequency variation due to the moisture is addressed by the lookup table that is stored in the μC memory. The reading of the prototype meter is compared to a commercial dew point meter. The comparison of the reading of the prototype meter with the electronic circuit is shown in Table 6. The frequency sensitivity and the nonlinearity of the sensor for 0–110 ppm moisture range are found to be 10.94 Hz/ppm and ~1% respectively. This is a linear, sensitive, low baseline drift and simple differential capacitive bridge circuit for converting the incremental capacitance change in the frequency with high resolution (1 ppm moisture) and accuracy (nearly 1%). However, because of the transformer, the circuit is not CMOS compatible and is suitable for the lossless capacitive sensor.

5.4 A Microcontroller Compatible Oscillator Based Active Bridge Circuit for Interfacing Capacitive Sensors

5.4.1 Working of the Circuit

An alternate form of the TRA bridge realized using the active devices are shown in Fig. 17a [41]. It combines the properties of the capacitance to frequency convertor

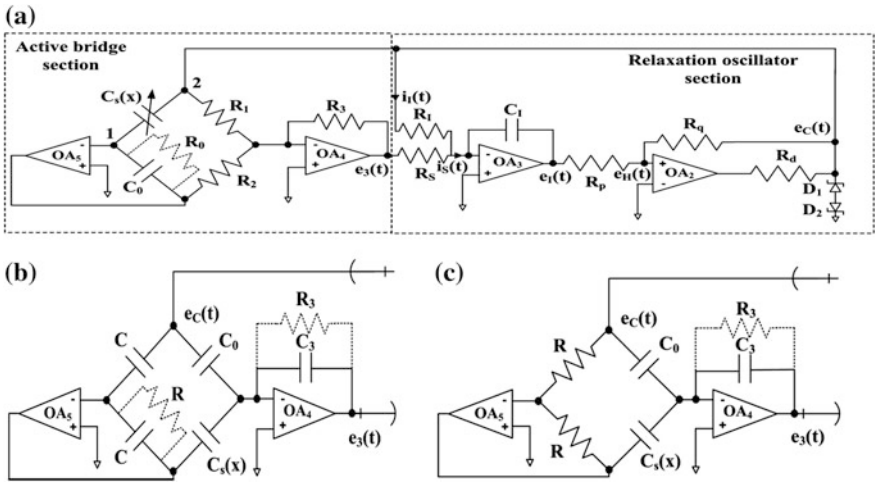

Fig. 17 **a**. The oscillator based active bridge for the capacitive sensor. **b** Full active bridge. **c** Half active bridge

and the capacitive ratio arm bridge technique with an output signal, which is compatible to the microcontroller [25, 32–34, 41]. The circuit offers all the features of the TRA bridge, including the CMOS compatibility. The circuit requires few hardware components and is easy to integrate for an application specific integrated circuit in a standard CMOS technology with configurable sensitivity. Figure 18 is the output waveforms. Element R_1, R_2, C_0 and $C_s(x)$ are the four arms of the bridge, which, along with the opamp OA_5 form an active bridge and, the opamp OA_4 forms a bridge amplifier. The operational amplifiers OA_2 and OA_3 work, as the integrator and the Schmitt trigger circuit of the relaxation oscillator respectively. The bridge is driven by the square wave voltage $e_C(t)$ (suitably scaled by diode clipper circuit) obtained from the output of OA_2. The bridge unbalanced voltage is amplified by an op-amp OA_4 to give the voltage, $e_3(t)$. This amplified voltage $e_3(t)$ and the voltage signal $e_c(t)$ are applied to the summing integrator of the oscillator. The frequency of the output waveform can be given by

$$f = f_o\left[1 + K_1\left\{\frac{C_s(x) - C_o}{C_o}\right\}\frac{R_I}{R_S}\right] \tag{22}$$

where, $f_0 = \frac{1}{K_2 R_I C_1\left(2+\alpha+\frac{1}{\alpha}\right)}$ is the central frequency at the balance condition when $\delta = 0$.

The capacitance of the humidity sensor can be written as

$$C_S(x) = C_o\left[1 + \frac{1}{K_1}\left\{\frac{f - f_o}{f_o}\right\}\frac{R_S}{R_I}\right] \tag{23}$$

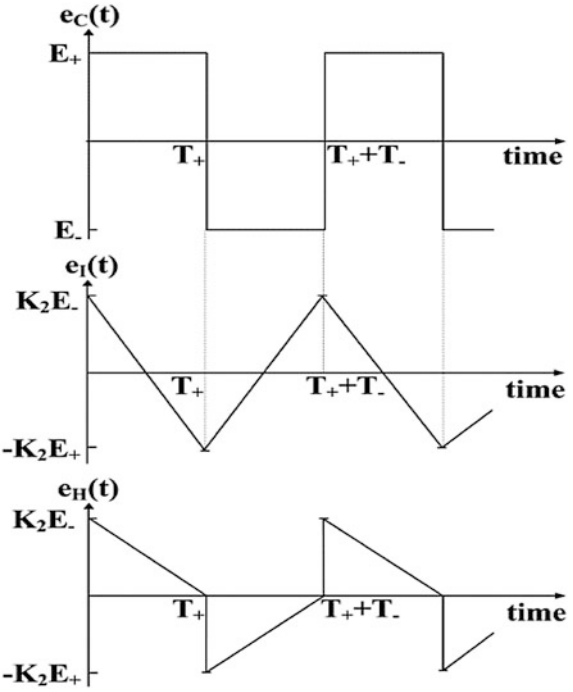

Fig. 18 Significant waveforms at different terminals

If C_x and C_0 are the two capacitors of a three electrode capacitive transducer, then the interface can be used to determine the relative permittivity of the dielectric medium, for example, the permittivity of edible oils or the transformer oil [15, 41]. To measure the permittivity of the dielectric using the interface, the relative permittivity can be given by

$$\in_r(x) = \left[1 + \frac{1}{K_1}\left(\frac{f - f_o}{f_o}\right)\frac{R_S}{R_I}\right] \tag{24}$$

$e_3(t) = e_C(t)\left\{\frac{C_s(X) - C_0}{C_3}\right\}$, for $sRC \gg 1$ and $sR_3C_3 \gg 1$ for the full active bridge and $e_3(t) = e_C(t)\left\{\frac{C_s(X) - C_0}{C_3}\right\}$, for $sR_3C_3 \gg 1$ for the half active bridge circuit.

5.4.2 Experimental Verification of the Interface Circuit

To confirm the performance as described, the circuit was hardware implemented by using the active devices having high slew rate, ultra-low offset voltage. Operational amplifier OP-07 was used for the integrator OA_3 and the amplifier OA_4, respectively and for the remaining op-amps, LF-351s were used. 2.7 V Zener diodes were

used for D_1 and D_2. For appropriate op-amp selection, the Gain Bandwidth Product (GBWP) should be a factor of approximately 100 times higher than the maximum oscillation frequency. The LF-351 op amp has a GBWP = 4 MHz (typ.) with Vs $= \pm 15$ V [29] and hence, the excitation frequency or the oscillator frequency should be below 40 kHz to achieve the satisfactory performance. The excitation frequency has been selected around 10 kHz. The oscillator frequency was adjusted to nearly 10 kHz by using the following component values: $R_1 = R_2 = 2.189\,k\Omega$, $R_3 = 0.976\,k\Omega$, $R_p = 1.108\,k\Omega$, $R_q = 2.227\,k\Omega$, $R_d = 100\,\Omega$, $R_I = 382\,k\Omega$, $C_s(x) = 500\,pF$, $C_I = 100\,pF$ and $C_0 = 500\,pF$. A high resistance value $R_0 = R_f = 10\,M\Omega$ was connected across the feedback capacitor that provides a dc current path due to the dc offset voltage and the bias current. Initially, the discrete capacitors were used in place of the capacitive sensor $C_s(x)$. Variation of the frequency with the discrete capacitance values with corresponding relative error is shown in Fig. 19. The maximum relative error of the capacitance value measured by the interface is found to be nearly 0.62%. The circuit is also tested with the capacitive sensors for the measurement of ppm level moisture and the dielectric constant of the edible oils respectively. The change in frequency of the circuit with the variation of the moisture in ppm is shown in Table 7. To determine the dielectric constant of the edible oils, the components values are redesigned to obtain the central frequency at 1 kHz. The capacitive sensor shown in Fig. 8c is used for the same. C_x is the capacitance with edible oil sample and C_0 is the free space air capacitor. The experiment has been performed for different samples of the oils. The percentage changes in frequency of the interface for the several identical samples of the oils are measured. The average dielectric constants of the sunflower and the mustard oil are ~3.15, ~2.95 and the percentage frequency changes are ~9.5% and 8.7% respectively. The effectiveness of the circuit for measuring the capacitance of the low value capacitive sensor is visible in the response. However, the circuit is suitable for interfacing the perfect capacitive sensor.

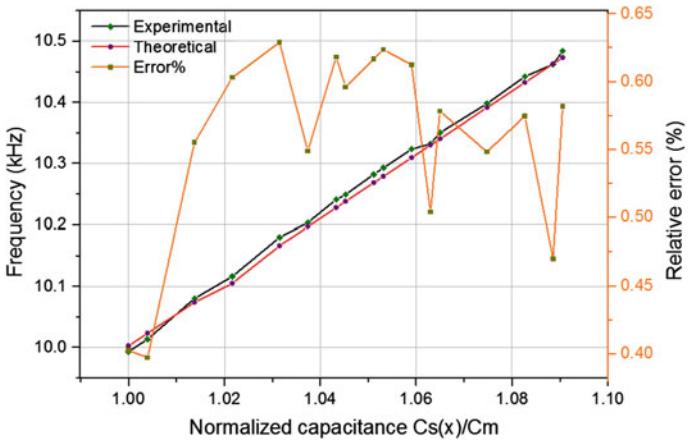

Fig. 19 Frequency output with the capacitance C_x

Table 7 Reading of the circuit with moisture concentration

Moisture (ppm)	Frequency (kHz)
4	9.99
13	10.12
29	10.20
50	10.28
60	10.32
70	10.35
81	10.4
90	10.44
100	10.48

5.5 An Impedance Measurement Technique for Wide-Range Lossy Capacitive Sensors

5.5.1 Working of the Interface

A new, simple and accurate impedance measurement technique (IMT) for wide range lossy capacitive sensor ('C_x' in parallel with 'R_x') based on the separation of in-phase and quadrature components of a modified active DeSauty bridge is discussed in this section [44]. The measurement range of the sensor parameters of the basic interface circuit can be improved further using an auto-balancing approach. In the auto balancing bridge, a voltage controlled variable reference capacitor, is connected at one arm of the active bridge, which forcefully nullifies the quadrature component of the output phase shifted signal. The phase difference of the output with respect to the input signal is zero only, when the voltage controlled capacitance is equal to the sensor capacitance, and at the same time, the output voltage of the interface circuit is proportional to the resistance component. Thus, at the quadrature component balance condition, the determination of C_x and R_x is possible. There are various circuits available in the literature for the measurement of the capacitance of the perfect capacitive sensors. Most of the reported works for the lossy sensors suffer from the complexity, the limited measurement range and the lower accuracy. In comparison to other techniques [34, 45–49], the advantages of the present interface circuit are; determination of R_x, C_x simultaneously; wide range of the components values; low base line drift; the stray capacitance immunity; low cost, capability of supplying same frequency signal to the sensor and the simplicity of the electronics. The phase and the amplitude of the output signal change due to the variation of the resistance and the capacitance of the sensor arm. The phase change of the output signal is converted into the time domain pulse wave modulated (PWM) signal using a phase sensitive detector as described in Fig. 14. Because of the lower output impedance of the opamp A1 and the virtual ground of the opamp A2, the output phase difference has negligible effect for the stray capacitances across the sensor arm. The phase difference has been extracted by applying V_i, V_o to the XOR gate through a zero crossing detector. The front-end of the first

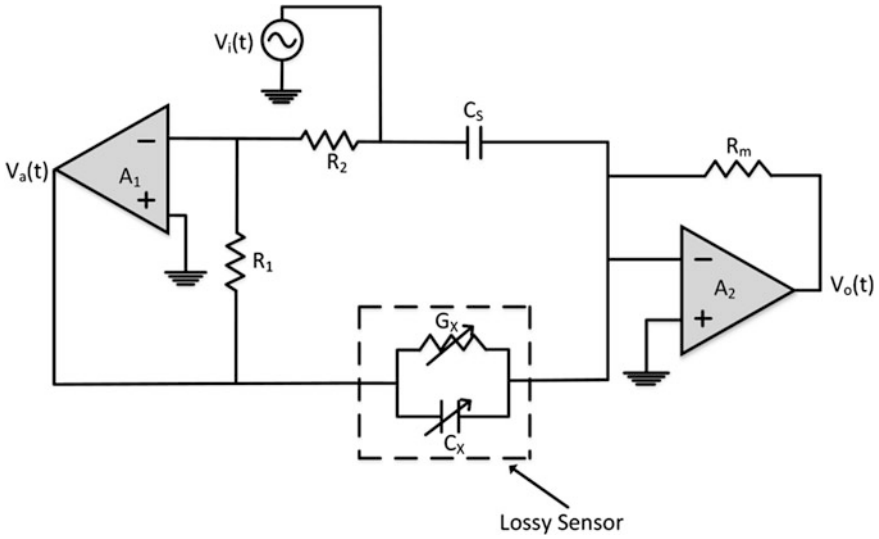

Fig. 20 The first basic impedance measurement circuit

proposed configuration is shown in Fig. 20, which is designed using the following elements: an inverting amplifier (A_1), a reference capacitance (C_s), a lossy capacitive sensor (C_x and G_x) and an amplifier (A_2). If the AC sinusoidal input voltage of the bridge, $V_i(t) = V_i \sin(\omega t)$, is applied to the input, then the output of the opamp A2, V_o can be written as

$$V_0(t) = R_m V_i(t)[(G_x + j\omega C_x) - (j\omega C_s)] \tag{25}$$

The Eq. (25) can be rewritten as

$$V_0[\cos\theta + j\sin\theta] = R_m V_i[(G_x) + j\omega(C_x - C_s)] \tag{26}$$

Separating real and imaginary parts of the Eq. (26), the values of R_x and C_x can be obtained as

$$R_x = \frac{V_i R_m}{V_o \mathrm{Cos}\theta} \; and \; C_x = \frac{V_o \mathrm{Sin}\theta}{V_i \, \omega \, R_m} + C_S \tag{27}$$

The phase difference θ can be converted into the time domain pulse wave signal using a XOR gate. The high output of the XOR gate 't_H' can be related with θ as

$$\frac{t_H}{T} = \frac{\theta}{2\pi}$$

where T is the time period, and the Eq. (27) can be finally expressed as:

$$C_x = \frac{V_o \mathrm{Sin}(2\pi f \cdot t_H)}{V_i R_m \omega} + C_S, \quad G_x = \frac{V_o \cos(2\pi f \cdot t_H)}{V_i R_m} \tag{28}$$

Thus, it is possible to estimate the values of the sensor parameters (C_x and R_x) from Eq. (28) by simply measuring the amplitude of the output voltage 'V_0' and HIGH state 't_H' of the PWM signal. This can be easily done by using a micro-controller or Lab VIEW software.

5.5.2 An Autobalance Active Bridge

The alternate form of the interface intended for improving the measurement range and the resolution is shown in Fig. 21. Only modification to the first circuit made is to obtain the voltage controlled variable capacitance C_s. In the modified circuit, a multiplier 'M', an amplifier 'A3' with gain 'A' and reference capacitance C_S form one arm of the bridge. The output of the amplifier A3 can expressed as

$$V_3 = \frac{V_i A K}{10} \tag{29}$$

where K is the variable DC voltage obtained from the DAC output. The voltage V_3 drives a current I_S through the reference capacitance C_s, while V_2 ($=-V_i$) causes a current I_x through the sensor arm. The unbalance current at the input of A_2 is converted into a voltage V_o. The output V_o can be written as

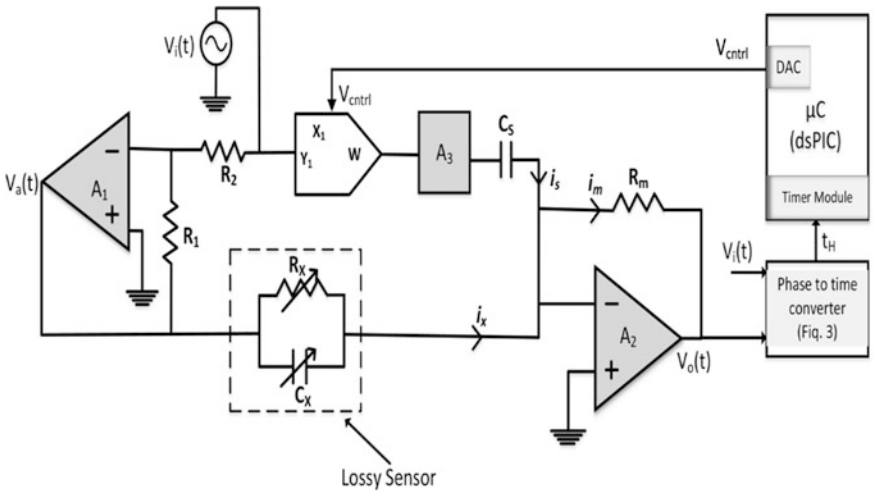

Fig. 21 Auto balancing active bridge for the impedance measurement

$$V_o = V_i R_m = \left[G_x + j\omega \left(C_x - \frac{KAC_s}{10} \right) \right],$$

$$\text{And, } [\theta = \tan^{-1} \left[\omega \left(C_x - \frac{KAC_s}{10} \right) \frac{1}{G_x} \right]$$

The phase difference θ in time domain at the output of the XOR gate can be written as $t_H = \frac{1}{2\pi f} \tan^{-1} \left[\omega \left(C_x - \frac{KAC_s}{10} \right) \frac{1}{G_x} \right]$. At balance condition, when t_H is zero, the C_x and R_x can be determined using the following expression:

$$C_x = \frac{V_{cntrl} A\ C_s}{10} \text{ and } R_x = R_m \frac{V_i}{V_0} \tag{30}$$

Smallest detectable capacitance can be given by $\Delta C_x = \frac{V_{DAC} A\ C_s}{2^n 10}$.

Where, ΔC_x is the smallest detectable capacitance change, n is the number of DAC bits, V_{DAC} is the reference voltage of DAC unit (=V_{ctrl}). For example, suppose we have a 10-bit DAC with an operating voltage range of 5 V, if we consider A = 10, and C_s = 10 pF, then the minimum detectable capacitance will be 0.0488 pF. In this sense, the readout operating range and the minimum detectable capacitance are directly related to V_{cntrl} value, which is in-turn depends on the number of DAC bits and the output voltage range of DAC. The electrical limit of the control voltage of the analog multiplier is 10 V, and the saturation level is 9.5 V. Since the output voltage of the multiplier is internally reduced by a factor of 10, so the gain of the non-inverting amplifier A_2 is selected according to the required resolution and the bandwidth.

5.5.3 Experimental Results of the First Electronic Circuit

The circuit shown in Fig. 20 was tested with the values; V_{in} = sin(ωt), f = 1 kHz, C_s = 100 pF, R_m = 480 kΩ. The ultra-low offset operational amplifier OPA-177 was used for A1, A2 and A3, the high slew rate operational amplifier LF351 was used for comparator O1 and O2 and the XOR gate HCF4070 was used for the phase detection purpose. The output of the XOR gate and the interface circuit were acquired in Lab-VIEW software using 'NI-ELVIS II' data acquisition (DAQ) card to simultaneously provide graphical user interface. Initial, discrete capacitive and parasitic resistive components are used for the sensor arm. All passive components have been first measured with an LCR meter (Agilent) and found to be ±2% tolerance for the resistive elements and ±3% tolerance for the capacitive elements.

The experimental results with the circuit for different values of the resistance from 68 to 10 MΩ and the capacitance from 200 pF to 1.1 nF is shown in Table 8. The maximum relative error is found to be 6%.

Table 8 Experimental results with discrete components

True value	R_x = 10 MΩ		R_x = 1 MΩ		R_x = 68 kΩ	
C_x (pF) (LCR meter)	C_x (pF) circuit	% error	C_x (pF) circuit	% error	C_x (pF) circuit	% error
200	195.3	−2.35	192.6	−3.7	189.2	−5.4
300	293.31	−2.23	291.9	−2.7	288.72	−3.76
400	395.12	−1.22	393.4	−1.65	386.8	−3.3
500	493.8	−1.24	491.7	−1.66	489.3	−2.14
600	595.70	−0.72	593.4	−1.1	592.5	−1.25
700	698.10	−0.27	696.43	−0.51	697.2	−0.4
800	803.4	0.43	801.36	0.17	806.64	0.83
900	906.09	0.68	906.48	0.72	919.17	2.13
1000	1009.2	0.92	1017.3	1.73	1035.8	3.58
1100	1114.85	1.35	1123.98	2.18	1147.08	4.28

Table 9 Experimental results with the autobalancing circuit

True value	R_x = 4.7 MΩ		R_x = 680 kΩ		R_x = 100 kΩ	
C_x (pF) (LCR meter)	C_x (pF) circuit	% error	C_x (pF) circuit	% error	C_x (pF) circuit	% error
100	96.8	−3.2	102.1	2.1	104.3	4.3
300	291.9	−2.7	302.79	0.93	312.6	4.2
600	586.32	−2.28	607.08	1.18	622.8	3.8
900	883.44	−1.84	909.09	1.01	934.38	3.82
1200	1178.64	−1.78	1223.04	1.92	1242	3.5
1500	1471.05	−1.93	1522.2	1.48	1556.1	3.74
1800	1781.1	−1.05	1834.56	1.92	1863.54	3.53
2000	2023	1.15	2061.2	3.06	2097.2	4.86

5.5.4 Experimental Results of the Autobalancing Bridge

To implement the autobalancing bridge, an analog multiplier 'AD633' [21] and a PIC microcontroller 'dsPIC33FJ16GS502' [22] operating at 40 MHz and having an inbuilt 10-bit DAC (3.3 V reference) were employed and the amplifier A3 with gain 30 was used to obtain the autobalance condition. The experiment was conducted with discrete resistance and capacitance having an enhanced range of capacitance (1.6 times of the previous range) and the resistance (3 times of the previous range). The results of the capacitance and resistance measurement are shown in Table 9. The maximum relative errors of the capacitance and the resistance measurement are 5% and 6% respectively. The minimum capacitance value of the autobalance technique is 50 pF. The minimum range can be increased further by using advanced opamps, high signal frequency and the high resolution DAC.

Table 10 Capacitance of the humidity sensor measured by the circuit

RH (%)	11	20	29	39	50	73	85	91
C_X (LCR meter)	70.0	71.9	74.9	81.7	91.1	302.5	576.2	782
Cx (meas)	65.4	66.4	70.7	78.2	87.4	313.6	589.1	798.3
% error	−6.5	−7.6	−5.7	−4.2	−4.2	3.7	2.2	2.1

Finally, the interface has been tested with the lossy capacitive type sensors like humidity sensor. The resistance value of the sensor varies in the range of 35 kΩ–4 MΩ and the capacitance value of the sensor varies in the range of 70–790 pF for the humidity range of 10–90% RH. The result of the humidity measurement is shown in Table 10.

5.6 *Current Mode Oscillator Circuit for the Grounded Capacitive Sensors*

Voltage mode oscillator combining the advantages of the bridge method of the capacitance measured has been discussed in Sects. 5.3 and 5.4. The voltage mode oscillator has the limited dynamic range because of the frequency dependent gain of the operational amplifiers which are utilized for the implementation of the circuit. This problem can be avoided by a current mode oscillator utilizing the second generation current conveyer (CCII). The current mode oscillator offers large dynamic range, wide bandwidth, high linearity, possibility of designing with low power consumption and simple analog circuit design. An oscillator based interface circuit for the grounded capacitive sensors with wide dynamic range using CCII has been discussed [51]. Its main operation is basically adopted from the voltage mode approach of current integration, and the configuration is designed in such a specific way that minimizes the effect of the parasitic components of CCIIs. The dynamic range has been improved by reducing the effect of the parasitic components at node X. This is done by avoiding the capacitive loads, keeping only grounded resistive load of slightly higher value than the parasitic resistance at the same terminal. In addition, it is also possible to set the circuit sensitivity and the operating frequency range externally, using the passive components. Simulation and the experimental results show a good agreement with the theoretical expectations with good linearity in the wide dynamic frequency range.

5.6.1 Current Conveyer Based Oscillator

Figure 22a shows the symbolic representation of a basic second generation current conveyer. The characteristics of the CCII can be described by the following equations

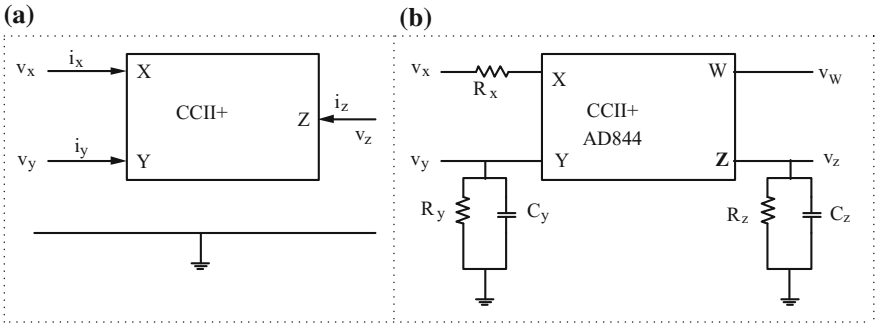

Fig. 22 **a** Symbol of the second generation current conveyer. **b** Analog device IC AD844 as a practical current conveyer

$$i_z = \pm \alpha_i i_x \ and \ v_x = v_y, i_y = 0 \tag{31}$$

The '±' symbol of current transfer ratio a_i indicates, whether the conveyor is framed as non-inverting or inverting circuits, labelled as CCII+ and CCII− respectively. The output current i_z depends on the input current i_x, which may be directly injected by applying the input voltage at X node, or by coping the input voltage from terminal Y. Analog device AD844 can be used as a CCII. The schematic diagram, of the practical AD844 as current conveyer is shown in Fig. 22b. The practical parasitic components values of the device are C_z = 4.5 pF, C_y = 2 pF, R_z = 3 MΩ, R_y = 10 MΩ and R_x = 50 Ω. The actual interface electronic circuit is shown in Fig. 23a where CCII+'A' works as a voltage to current converter and CCII+'B' works as a hysteresis comparator. The important waveforms at different nodes are shown in Fig. 23b. Considering the ideal conditions of the conveyer, the peak to peak voltage, v_{02} can be written as

$$v_{02}(p-p) = V_s\left(\frac{R_2 - R_1}{R_2}\right) \tag{32}$$

The voltage across the capacitor due to current i_{XB} can be expressed as

$$v_{02}(p-p) = \frac{V_s}{2R_xC_x}T \tag{33}$$

Comparing (32) and (33), the time period of the oscillator output can be written as

$$T = 4R_xC_x\frac{R_2 - R_1}{R_2} \tag{34}$$

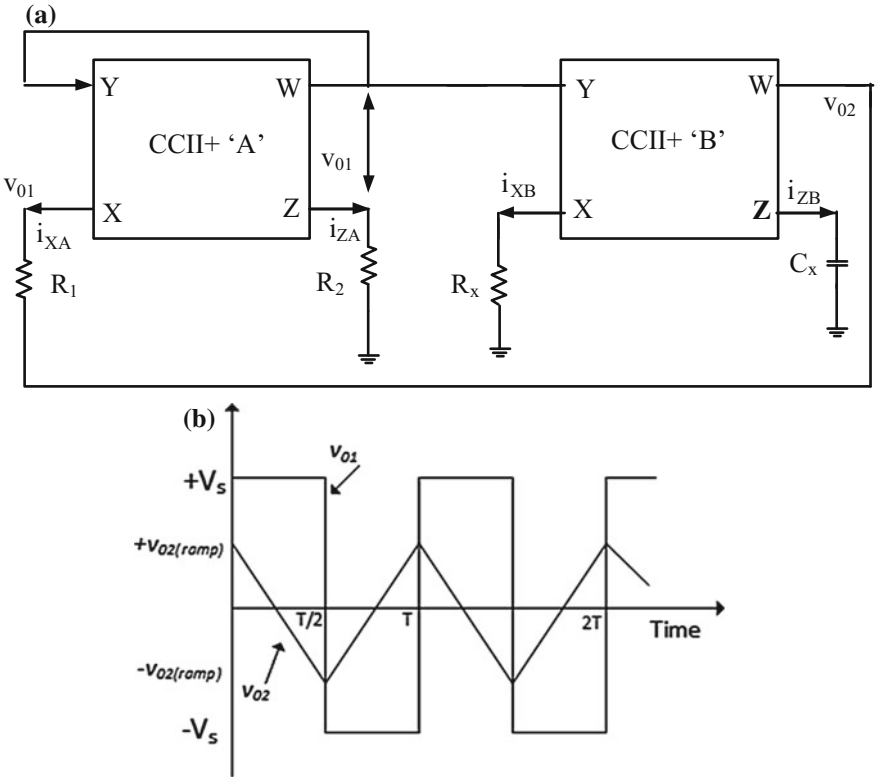

Fig. 23 **a** Current conveyer based interface electronics circuit, **b** waveforms at important nodes

If we consider the parasitic components of the device AD844, the time period can be written as

$$T = 4(R_x + R_{XB})C_x \frac{R_2 - (R_1 + R_{XA})}{R_2} \tag{35}$$

Time period is depending on both the values of R_x and C_x.

5.6.2 Experimental Verification of the Interface Circuit

The circuit shown in Fig. 23a was first simulated by varying C_X and R_X keeping $R_1 = 6.8$ kΩ and $R_2 = 10$ kΩ. The simulation results are shown in Tables 11 and 12. The range of the oscillation frequency for the variation of the capacitance from 50 pF to 500 nF is 850 kHz to 99 Hz, very wide.

The circuit was also hardware implemented on the breadboard with the components values $R_1 = 6.8$ kΩ, $R_2 = 10$ kΩ and $Rx = 40$ kΩ. The oscillation frequency in the range of 0–250 kHz was measured with the variation of the

Table 11 Time period of the oscillator with the variation of C_x

R_x = 20 kΩ			
C_x (pF)	Theoretical time period (μs)	Measured time period (μs)	Relative error (%)
50	1.08	1.14	5.56
500	10.11	10.42	3.74
5000	108	102	5.80
50,000	1080	1020	5.54
500,000	10800	10100	6.48

Table 12 Time period of the oscillator with the variation of R_x

C_x = 50 pF			
R_x (kΩ)	Theoretical time period (μs)	Measured time period (μs)	Relative error (%)
10	2.56	2.70	5.18
100	5.31	5.40	1.67
500	27.54	27.01	1.96
1000	57.57	54.05	6.11
2000	119.47	107.41	10.09

Table 13 Comparison of the circuit with other similar circuits

Characteristics	Frequency range (Hz–kHz)	Active components	Passive components	Output signal	Prototyping and experimental
Double CCII(+) based oscillator [51]	100–850	Two	Four	Square and triangular wave	Yes
CCII(+) based design [52]	25–225	Two	Four	Square and triangular wave	Yes
CMOS/CCII(+) differentiation Based [53]	0.128–737	Two	Six	Square	Yes
CMOS based design [54]	25–260	Two	Two	Square	No
CCII(+) based design [55]	100–100	One	Four	Square/Triangular	Yes

capacitance, *Cx* from 100 pF to 200 nF. The maximum relative error of the measured oscillation frequency of the output signal with respect to the theoretical value is nearly 8%. Similarly, the oscillation frequency was also measured with the variation of R_x from 50 kΩ to 1.5 MΩ for the components values of C_x = 100 pF, R_1 = 7.4 kΩ, R_2 = 10 kΩ. The maximum relative error of the actual frequency with respect to the theoretical value is 9%. Finally, a comparison table showing the performance of the current mode oscillator circuit with other existing similar circuits for the capacitive and the resistive sensors is shown in Table 13. The circuit based on charging/discharging effect of resistance-capacitance (RC) cell, is having a simple circuit topology requiring two CCIIs and four passive components only.

6 Conclusions

Capacitive sensors both perfect and lossy are widely used for the measurement of different physical and chemical parameters. The preference and the uses of such type of the capacitive sensors are getting more importance day by day with the needs of new information to be measured efficiently and reliably. The capacitive sensors can be useful sometimes for the hassle free non-contact measurement of the physical parameters. Different types of the capacitive sensors suitable for the measurement of the parameters are discussed. Though the cross-capacitance is used as primary capacitance standards for different national laboratories, its potential is yet to be exploited fully for sensing applications. The capacitive sensor needs extra precautions to avoid the errors due to stray effects, particularly for the low capacitance measurement. Issues related to the development of the interface electronic circuit for the sensors are also discussed. Some advanced interface electronic circuits for both the perfect and the lossy capacitive sensors are discussed. These interface circuits are promising for interfacing different capacitive sensors with the ability to minimize the stray capacitances, where the capacitance values vary widely.

References

1. J. Fraden, *Handbook of Modern Sensors, Physics, Design, and Applications* (Springer, New York, 2003)
2. E. Doeblin, D.N. Manik, *Measurement Systems, Applications and Design*, 5th edn. (Tata Macgraw Hill, New Delhi, 2007)
3. A. De Marcellis, G. Feri, *Analog Circuits and Systems for Voltage Mode and Current Mode Sensor Interfacing Applications* (Springer, 2011)
4. A. Abu-Al-Aish, M. Rehman, Development of a capacitive mass measuring system. Sens. Actuators A **151**, 113–117 (2009)
5. B. Hague, T.R. Ford, *Alternating Current Bridge Methods,* 6th edn. (Pitman Publishing, 1971)
6. Z.M. Rittersma, Recent achievements in miniaturized humidity sensors—a review of transduction techniques. Sens. Actuators A **96**, 196–2002 (2002)
7. T.A. Blanka, L.P. Eksperiandova, K.N. Belikov, Recent trends of ceramic humidity sensors development: a review. Sens. Actuators B **228**, 416–442 (2016)
8. S. Dhanekar, S.S. Islam, T. Islam, A.K. Shukla, Harsh, Organic vapour sensing by porous silicon: influence of molecular kinetics in selectivity studies. Phys. E (Elsevier) **42**(5), 1648–1652 (2010)
9. T. Islam, H. Saha, S.S. Islam, Porous silicon based sensor array for ethanol sensing. Sens. Lett. **7**, 1077–1085 (2009)
10. Golding, Widdies, *Electrical Measurements and Measuring Instruments*, 5th edn. (Reem Publication, 2009)
11. F.N. Toth, D. Bertels, G.C.M. Meijer, A low cost, stable reference capacitor for capacitor sensor systems. IEEE Trans. Instrum. Meas. **45**(2), 526–530 (1996)
12. M. Rehman, S.K. Mukherjee, V.G.K. Murti, Effect of a symmetrically placed dielectric on the capacitance of a cylindrical cross-capacitor. Proc. IEE (England) **129**(5) (1982)

13. W.Ch. Herrens, Applications of capacitance techniques in sensor design. J. Phys. E: Sci. Instrum. **19**, 897–906 (1986)
14. F. Reverter, X. Liand, G.C.M. Meijer, Stability and accuracy of active shielding for grounded capacitive sensors. Meas. Sci. Technol. **17,** 2884–2890 (2006)
15. A.U. Khan, T. Islam, J. Akhtar, An oscillator-based active bridge circuit for interfacing capacitive sensors with microcontroller compatibility. IEEE Trans. Instrum. Meas. (2016)
16. T. Islam, Md.R. Mahboob, S.A. Khan, A simple MOX vapor sensor on polyimide substrate for measuring humidity in ppm level. IEEE Sens. J. **15**(5), 3004–3013 (2015)
17. T. Islam, A.T. Nimal, U. Mittal, M.U. Sharma, A micro interdigitated thin film metal oxide capacitive sensor for measuring moisture in the range of 175–625 ppm. Sens. Actuators B **221**, 357–364 (2015)
18. T. Islam, M.Z.U. Rahman, Investigation of the electrical characteristics on measurement frequency of a thin-film ceramic humidity sensor. IEEE Trans. Instrum. Meas. **65**(3) (2016)
19. A.I. Zia, M.S.A. Rahman, S.C. Mukhopadhyay, et al., Technique for rapid detection of phthalates in water and beverages. J. Food Eng. **116,** 515–523 (2013)
20. T. Yin, W. Wei, L. Yang, X. Gao, Y. Gao, A novel capacitive immunosensor for transferrin detection based on ultrathin alumina sol–gel-derived films and gold nanoparticles. Sens. Actuators B **117**, 286–294 (2006)
21. A. Abu-Al-Aish, R. Mahfoozur, A.H.A. Hassan, M.R. Arshad, Development of an intelligent capacitive mass sensor based on co-axial cylindrical capacitor. J. Sens. Transducers, **105**(6), 1–9 (2009)
22. M. Rehman, V.G.K. Murti, A sensitive and linear pressure transducer. J. Phys. E: Sci. Instrum. (England) **14**, 988–992 (1981)
23. E. Basheer, M.M. Rahman, A novel capacitive rotation speed transducer. Meas. Sci. Technol. **13**, 2027–2031 (2002)
24. Z. Chen, C. Lu, Humidity sensors: a review of materials and mechanisms. Sens. Lett. **3**, 274–295 (2005)
25. S.M. Huangt, A.L. Stottf, R.G. Green, M.S. Beck, Electronic transducers for industrial measurement of low value capacitances. J. Phys. E: Sci. Instrum. **21**, 212–250 (1988)
26. G.C.M. Meijer, *Smart Sensor Systems* (Wiley, Delft, The Netherlands, 2008), pp. 240–241
27. M. Rehman, M.T. Ahmad, V.G.K. Murti, A TRA bridge technique for in-circuit impedance measurement. IEEE Trans. Instrum. Meas. (USA) **IM-33**, 252–256 (1984)
28. A. Ashrafi, H. Golnabi, A high precision method for measuring very small capacitance changes. Rev. Sci. Instrum. **70**(8), 3483–3487 (1999)
29. A. De Marcellis, G. Ferri, E. Palange, A novel analog autocalibrating phase-voltage converter for signal phase-shifting detection. IEEE Sens. J. **11**(2), 259–266 (2011)
30. H. Binxin, J. Wang, G. Song, F. Zhang, A compact wideband precision impedance measurement system based on digital auto-balancing bridge. Meas. Sci. Technol. **27**, 055902–055915 (2016)
31. R. Rybski, J. Kaczmarek, K. Kontorski, Impedance comparison using unbalanced bridge with digital sine wave voltage sources. IEEE Trans. Instrum. Meas. **64**(12), 3380–3386 (2016)
32. A. De Marcellis, G. Ferri, P. Mantenuto, Uncalibrated operational amplifier-based sensor interface for capacitive/resistive sensor applications. IET Circuits Devices Syst. **9**(4), 249–255 (2015)
33. S.N. Nihtianov, G.P. Shterev, B. Iliev, G.C.M. Meijer, An interface circuit for R–C impedance sensors with a relaxation oscillator. IEEE Trans. Instrum. Meas. **50**(6), 1563–1567 (2001)
34. Y. Liu, S. Chen, M. Nakayama, K. Watanabe, Limitations of a relaxation oscillator in capacitance measurements. IEEE Trans. Instrum. Meas. **49**(5), 980–983 (2000)
35. P. Mantenuto, A. De Marcellis, G. Ferri, Novel modified De-Sauty autobalancing bridge-based analog interfaces for wide-range capacitive sensor applications. IEEE Sens. J. **14**(5), 1664–1672 (2014)
36. N. Madhu Mohan, V. Jagadeesh Kumar, Novel signal conditioning circuit for push-pull type capacitive transducers. IEEE Trans. Instrum. Meas. **56**(1), 153–157 (2007)

37. D. Wang, Fdc1004: basics of capacitive sensing and applications, Texas Instruments, Dallas, TX, USA, Appl. Rep. SNOA927, 2014
38. T. Islam, K.K. Mistry, K. Sengupta, H. Saha, Measurement of gas moisture in the ppm range by porous silicon (PS) and porous alumina sensors. Int. J. Sens. Mater. **16**(7), 345–356 (2004)
39. T. Islam, Md.F. Khan, S.A. Khan, H. Saha, A sensitive digital moisture detector for Nanostructured thin film sensor. Int. J. Smart Sens. Intell. Syst. **7**(3), 1059–1076 (2014)
40. T. Islam, S.A. Khan, Md.F.A. Khan, S.C. Mukhopadhyay, A relaxation oscillator based transformer ratio arm bridge circuit for capacitive humidity sensor. IEEE Trans. Instrum. Meas. **67**(12), 3414–3422 (2015)
41. T. Islam, A.U. Khan, J. Akhtar, M.Z.U. Rahman, A digital hygrometer trace moisture measurement. IEEE Trans Indus. Electron. **61**(10), 5599–5605 (2014)
42. H. Shibata, M. Ito, M. Asakursa, K. Watanabe, A digital hygrometer using a polyimide film relative humidity sensor. IEEE Trans. Instrum. Meas. **45**(2), 564–588 (1996)
43. T. Islam, L. Kumar, S.A. Khan, A novel sol-gel thin film porous alumina based capacitive sensor for measuring trace moisture in the range of 2.5 to 25 ppm. Sens. Actuators B, **173**, 377–384 (2012)
44. S. Malik, K. Kishore, T. Islam, Z.H. Zargar, S.A. Akbar, A time domain bridge-based impedance measurement technique for wide-range lossy capacitive sensors. Sens. Actuators A **234**, 248–262 (2015)
45. A.D. Ferri, C. Marcellis, V. Di Carlo, A. Stornelli, A. Flammini, D. Depari, E. Marioli, A CCII-based low-voltage low-power read-out circuit for DC-excited resistive gas sensor. IEEE Sens. J. **9**(12), 2035–2041 (2009)
46. S.Y. Yurish, N.V. Kirianaki, Interfacing circuit design for frequency-time domain MEMS sensors, in *International MEMS Conference* (2006)
47. S.C. Bera, J.K. Ray, S. Chattopadhyay, A low-cost non-contact capacitance-type level transducer for a conducting liquid. IEEE Trans. Instrum. Meas. **55**, 778–786 (2006)
48. Analog Devices, Norwood, MZ, USA. Datasheet, AD5933, 12-BitImpedance Converter [Online], http://www.analog.com/media/en/technical-documentation/data-sheets/AD5933.pdf (2013)
49. C. Kolle, P. O'Leary, Low cost, high precision measurement system for capacitive sensors. Meas. Sci. Technol. **9**(3), 510–517 (1998)
50. F. Reverter, O. Casas, A microcontroller-based interface circuit for lossy capacitive sensors. Meas. Sci. Technol. **21**, 65203–65211 (2010)
51. S. Malik, D. Sharma, K. Kishore, M. Maharana, S.A. Akbar, T. Islam, A CCII-based wide frequency range square/triangular wave generator, in *2015 IEEE 2nd International Conference on Recent Trends in Information Systems July 9–11, 2015, Jadavpur University, Kolkata, India*
52. D. Pal, A. Srinivasulu, B.B. Pal, A. Demosthenous, B.N. Das, Current conveyor-based square/triangular waveform generators with improved linearity. IEEE Trans. Instrum. Meas. **58**(7), 2174–2180 (2009)
53. A.D. Marcellis, C.D. Carlo, G. Ferri, V. Stornelli, A CCII-based wide frequency range square waveform generator. Int. J. Circuit Theory Appl. **41**, 1–13 (2013)
54. S.D. Re, A.D. Marcellis, G. Ferri, V. Stornelli, Low voltage integrated astable multivibrator based on a single CCII, *in IEEE Proceedings—Prime* (Bordeaux, France, 2007)
55. M. Abuelma'atti, S. Al-Shahrani, New CFOA-based trinagular/square wave generator. Int. J. Electron. **84**, 583–588 (1998)